

## Supplementary information

### Towards the practical realization of high-performance Ag<sub>2</sub>Se-based thermoelectric coolers

Feng Jiang<sup>a†</sup>, Zhengtao Wang<sup>a†</sup>, Wen Zhong<sup>a</sup>, Yifan Zhou<sup>a</sup>, Zhengyang Zhou<sup>a</sup>, Longzhi Wu<sup>a</sup>, Jiang Chen<sup>a</sup>, Yao Xu<sup>a</sup>, Xiaodong Wang<sup>a,d</sup>, Feng Cao<sup>c</sup>, Qian Zhang<sup>a, b, e\*</sup>, and Jun Mao<sup>a, b, e\*</sup>

*a School of Materials Science and Engineering, and Institute of Materials Genome & Big Data, Harbin Institute of Technology (Shenzhen), Shenzhen 518055, P.R. China.*

*b State Key Laboratory of Precision Welding & Joining of Materials and Structures, Harbin Institute of Technology, Harbin 150001, P.R. China.*

*c School of Science, Harbin Institute of Technology (Shenzhen), Shenzhen 518055, P.R. China.*

*d Institute of Special Environments Physical Sciences, Harbin Institute of Technology (Shenzhen), Shenzhen 518055, P.R. China.*

*e School of Materials Science and Engineering, Shenzhen Key Laboratory of New Materials Technology, Shenzhen 518055, P.R. China.*

<sup>†</sup>These authors contributed equally to this work.

\*Corresponding authors, email: zhangqf@hit.edu.cn; maojun@hit.edu.cn;

## Contents

1. Setting parameters for the finite element simulation of  $\text{Ag}_2\text{Se}$ -based cooler
2. Sample density of  $\text{Ag}_2\text{Se}$  materials with different sizes
3. Specific heat capacity of the  $\text{Ag}_2\text{Se}$  sample
4. Energy dispersive spectroscopy mapping of the  $\text{Ag}_2\text{Se}$  sample
5. Hall carrier concentration and mobility of the  $\text{Ag}_2\text{Se}$  sample
6. The lattice thermal conductivity of the  $\text{Ag}_2\text{Se}$  sample
7. Thermoelectric properties of five  $\text{Ag}_2\text{Se}$  samples
8. Contact resistivity of the soldered  $\text{Ag}/\text{Ag}_2\text{Se}$  joint
9. Energy dispersive spectroscopy and linear scanning of the  $\text{Ag}/\text{Ag}_2\text{Se}$  interface
10. Linear energy dispersive spectroscopy scanning of the  $\text{Ag}/\text{SnBi}$  interface
11. Comparison of thermoelectric cooling performance for  $\text{Ag}_2\text{Se}$ ,  $\text{Bi}_2\text{Te}_3$ , and  $\text{Mg}_3(\text{Sb}, \text{Bi})_2$ -based devices at the hot-side temperature of 300 K
12. The simulated cooling performance of the 7 pairs  $\text{Ag}_2\text{Se}/(\text{Bi}, \text{Sb})_2\text{Te}_3$  thermoelectric cooler
13. Thermoelectric cooling performance of the  $\text{Ag}_2\text{Se}$ -based cooler at the hot-side temperature of 325 K
14. Coefficient of performance as a function of the electrical current of the  $\text{Ag}_2\text{Se}$ -based thermoelectric cooler
15. Interfacial properties of the  $\text{Ag}_2\text{Se}$ -based thermoelectric cooler after cycling

## I. Setting parameters for the finite element simulation of Ag<sub>2</sub>Se-based cooler

Table S1. Finite element simulation setting parameters.

Parameter	Value
Cross-sectional area of the Ag <sub>2</sub> Se legs	$1.8 \times 1.8 \text{ mm}^2$
Height of the Ag <sub>2</sub> Se legs	2.5 mm
Cross-sectional area of the (Bi, Sb) <sub>2</sub> Te <sub>3</sub> legs	$2.0 \times 2.0 \text{ mm}^2$
Height of the (Bi, Sb) <sub>2</sub> Te <sub>3</sub> legs	2.5 mm
Thickness of copper electrode	0.065 mm
Thickness of Al <sub>2</sub> O <sub>3</sub> substrate	0.38 mm
The area of the Al <sub>2</sub> O <sub>3</sub> substrate of the cold side	$13.0 \times 13.0 \text{ mm}^2$
The area of the Al <sub>2</sub> O <sub>3</sub> substrate of the hot side	$13.0 \times 16.0 \text{ mm}^2$
Thermal conductivity of the substrate	$20 \text{ W m}^{-1} \text{ K}^{-1}$
Thermal conductivity of the thermal grease	$4.8 \text{ W m}^{-1} \text{ K}^{-1}$
Heat load	0.0-2.5 W
Hot-side temperature	300 K
Contact resistivity of Ag <sub>2</sub> Se legs	$5.0 \mu\Omega \text{ cm}^2$
Contact resistivity of (Bi, Sb) <sub>2</sub> Te <sub>3</sub> legs	$5.0 \mu\Omega \text{ cm}^2$

## 2. Sample density of Ag<sub>2</sub>Se materials with different sizes

**Table S2.** Sample density of Ag<sub>2</sub>Se materials with different sizes

Sample diameter (mm)	Measured density (g cm <sup>-3</sup> )	Relative density (%)
10.0	8.05	98.17
12.7	8.07	98.41
20.0	8.03	97.93
25.4	8.06	98.29

### 3. Specific heat capacity of the $\text{Ag}_2\text{Se}$ sample

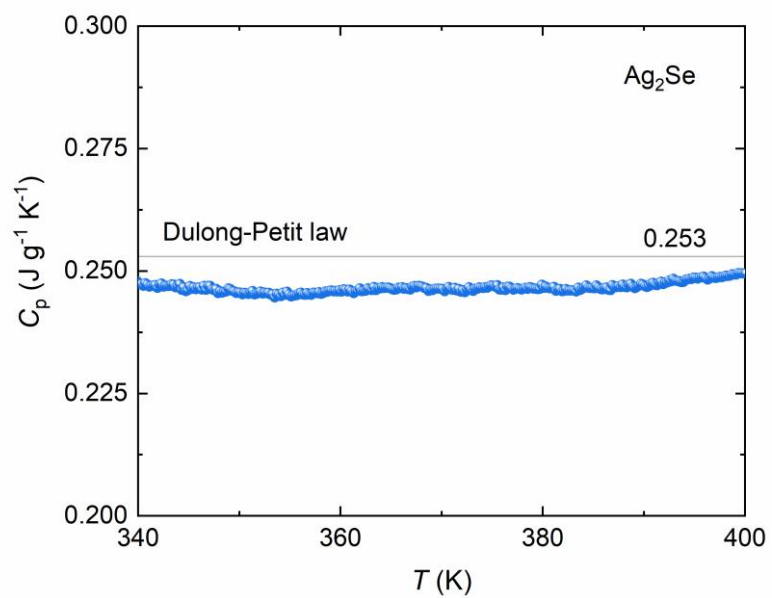


**Figure S1.** Specific heat capacity of the  $\text{Ag}_2\text{Se}$  sample.

#### 4. Energy dispersive spectroscopy mapping of the $\text{Ag}_2\text{Se}$ sample

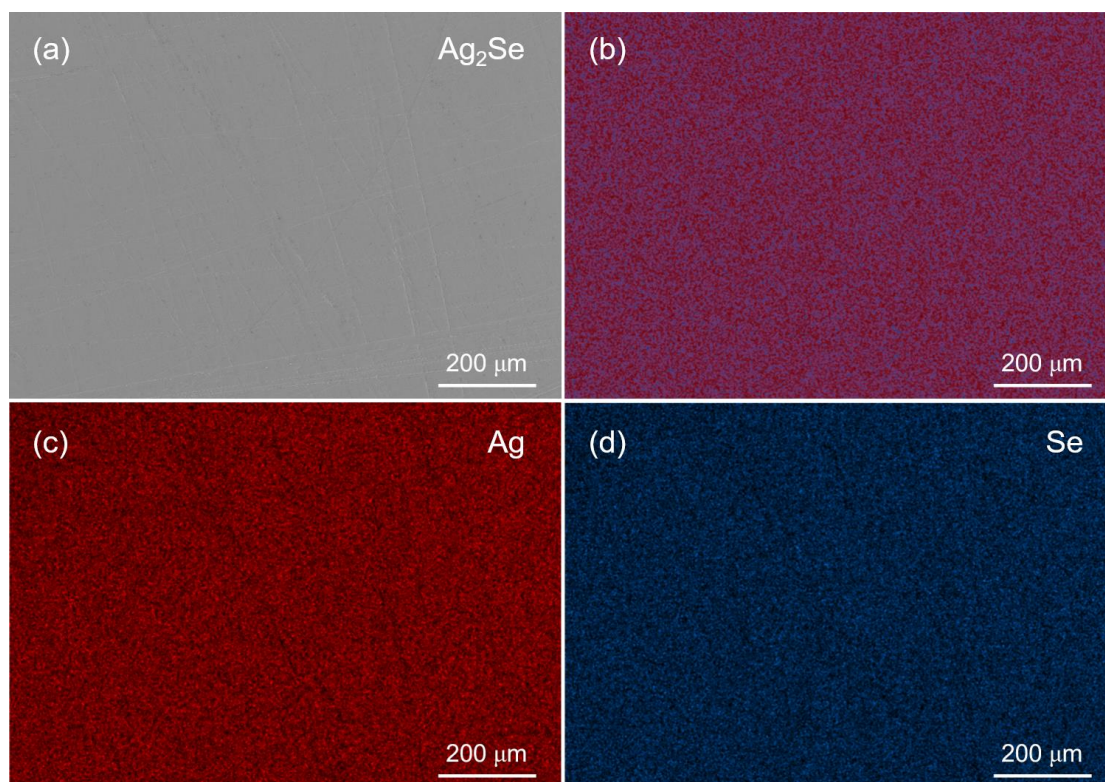


**Figure S2.** (a) Surface morphology, and (b-d) energy dispersive spectroscopy mapping of the  $\text{Ag}_2\text{Se}$  sample.

## 5. Hall carrier concentration and mobility of the $\text{Ag}_2\text{Se}$ sample

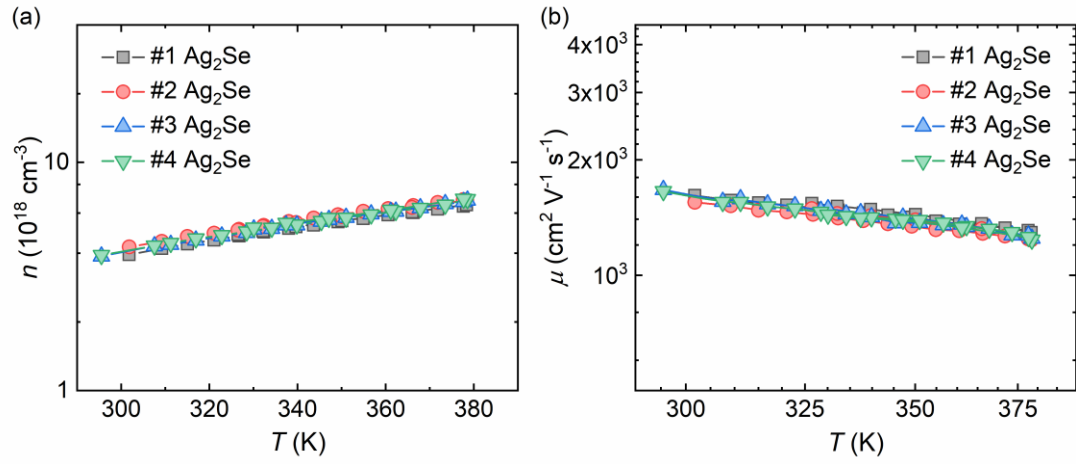


**Figure S3. Hall carrier concentration and mobility of the  $\text{Ag}_2\text{Se}$  sample.** (a) Carrier concentration. (b) Carrier mobility.

## 6. The lattice thermal conductivity of the Ag<sub>2</sub>Se sample

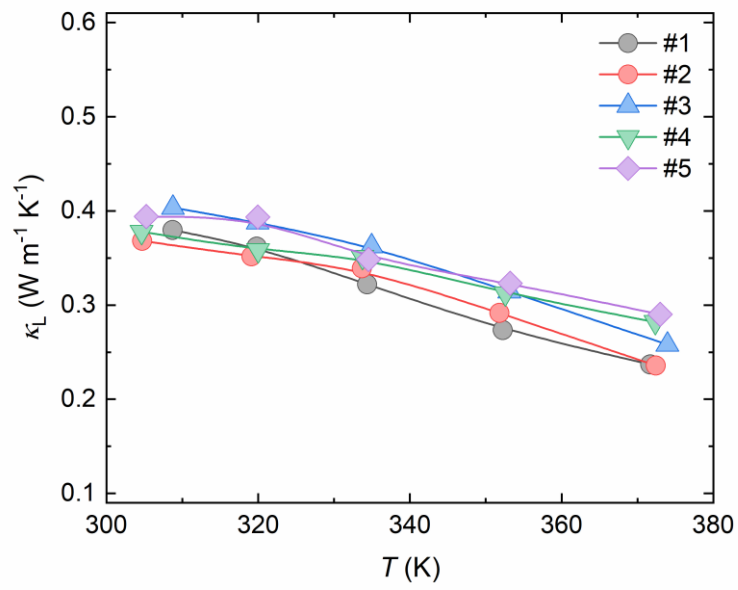


**Figure S4.** The lattice thermal conductivity of the Ag<sub>2</sub>Se sample.



## 7. Thermoelectric properties of the $\text{Ag}_2\text{Se}$ samples

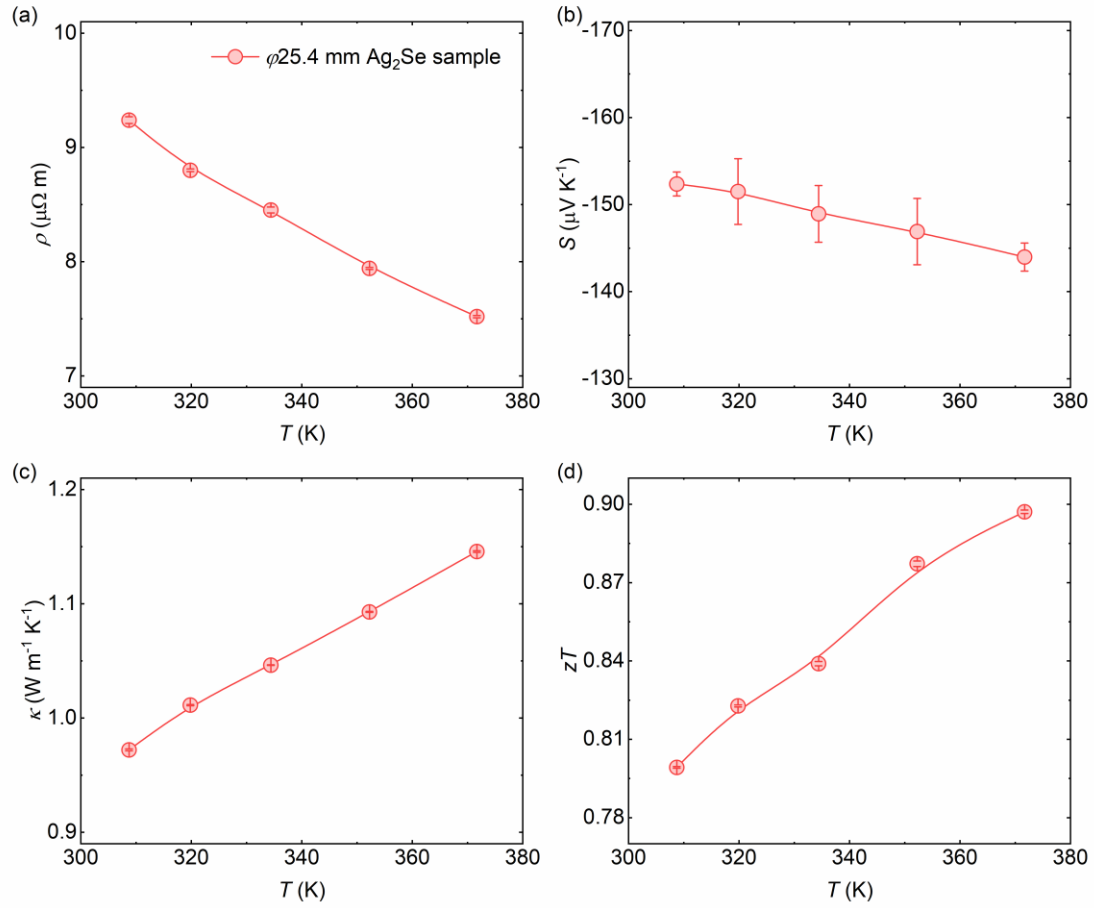


**Figure S5. Thermoelectric properties of the  $\text{Ag}_2\text{Se}$  samples.** Temperature-dependent (a) electrical resistivity, (b) Seebeck coefficient, (c) thermal conductivity, and (d)  $zT$  values.

### 8. Contact resistivity of the soldered Ag/Ag<sub>2</sub>Se joint

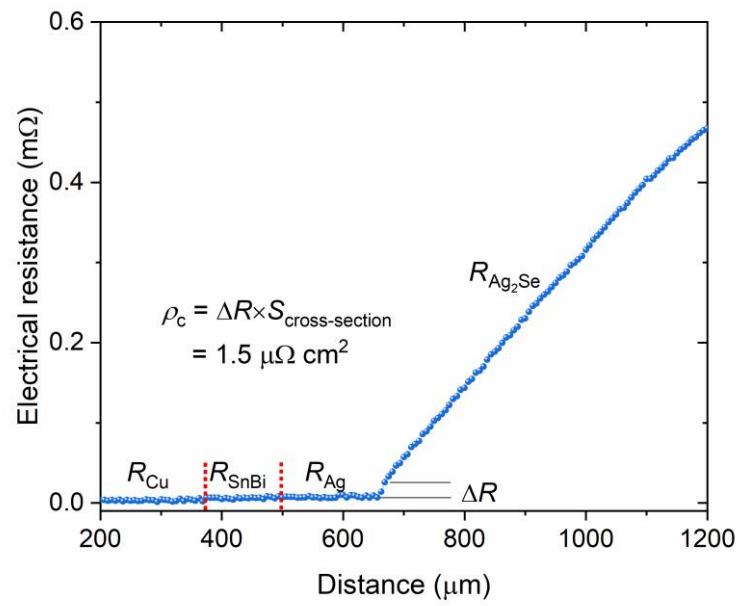


**Figure S6.** Contact resistivity of the soldered Ag/Ag<sub>2</sub>Se joint.

## 9. Energy dispersive spectroscopy and linear scanning of the Ag/Ag<sub>2</sub>Se interface

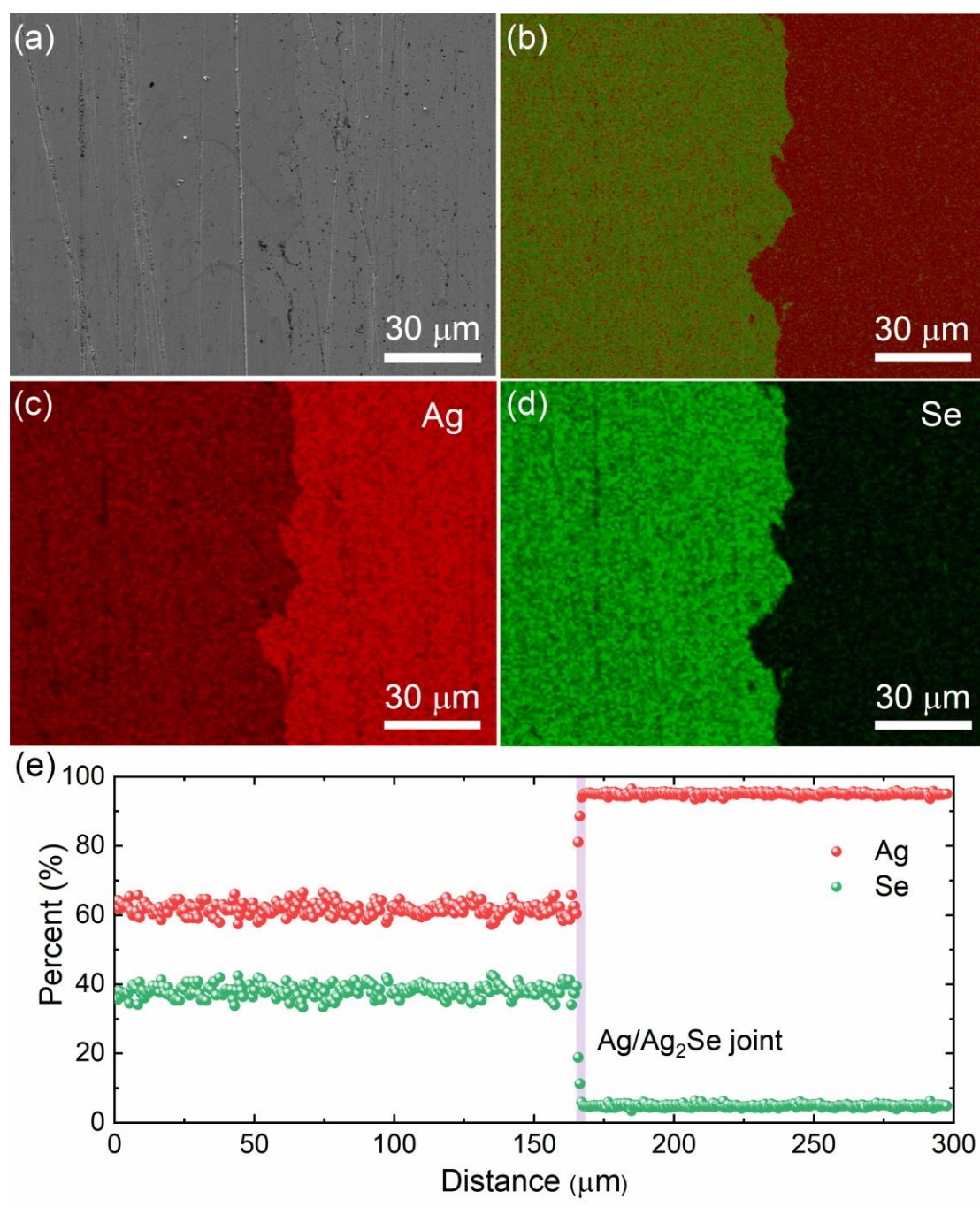


**Figure S7.** (a) The Ag/Ag<sub>2</sub>Se interface and (b-d) corresponding EDS mapping for the interface. (e) Linear EDS scanning across the Ag/Ag<sub>2</sub>Se interface.

## 10. Linear energy dispersive spectroscopy scanning of the Ag/SnBi interface

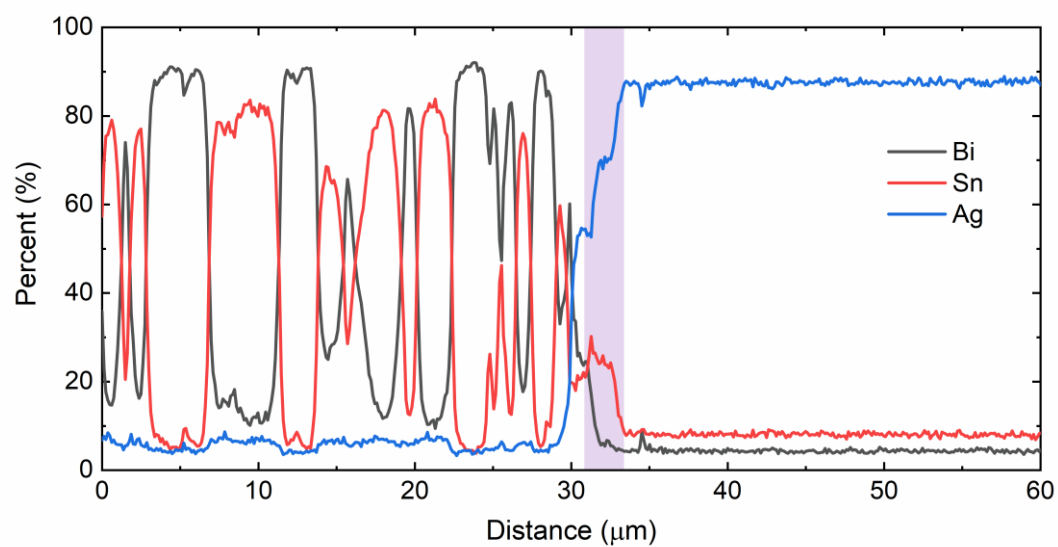


**Figure S8.** Linear EDS scanning across the Ag/SnBi solder interface.

# 11. Comparison of thermoelectric cooling performance for Ag<sub>2</sub>Se, Bi<sub>2</sub>Te<sub>3</sub>, and Mg<sub>3</sub>(Sb, Bi)<sub>2</sub>-based devices at the hot-side temperature of 300 K

**Table S3.** Comparison of thermoelectric cooling performance for Ag<sub>2</sub>Se, Bi<sub>2</sub>Te<sub>3</sub>, and Mg<sub>3</sub>(Sb, Bi)<sub>2</sub>-based devices at the hot-side temperature of 300 K

n-type leg	p-type leg	Cooling temperature difference (K)	Cooling power density (W cm <sup>-2</sup> )	Reference
Ag <sub>2</sub> Se	Bi <sub>2</sub> Te <sub>3</sub> alloys	55.4	1.5	This work
Ag <sub>2</sub> Se	Bi <sub>2</sub> Te <sub>3</sub> alloys	57.7	1.5	Jiang <i>et al.</i> <sup>[1]</sup>
Ag <sub>2</sub> Se	Bi <sub>2</sub> Te <sub>3</sub> alloys	56.0	1.4	Liu <i>et al.</i> <sup>[2]</sup>
Ag <sub>2</sub> Se	MgAgSb	52.0	0.8	Zhao <i>et al.</i> <sup>[3]</sup>
Bi <sub>2</sub> Te <sub>3</sub>	Bi <sub>2</sub> Te <sub>3</sub> alloys	70.1	1.6	Sun <i>et al.</i> <sup>[4]</sup>
Bi <sub>2</sub> Te <sub>3</sub>	Bi <sub>2</sub> Te <sub>3</sub> alloys	73.9	2.2	Zhao <i>et al.</i> <sup>[5]</sup>
Mg <sub>3</sub> (Sb, Bi) <sub>2</sub>	Bi <sub>2</sub> Te <sub>3</sub> alloys	69.0	1.3	Ma <i>et al.</i> <sup>[6]</sup>
Mg <sub>3</sub> (Sb, Bi) <sub>2</sub>	MgAgSb	52.0	0.8	Xie <i>et al.</i> <sup>[7]</sup>
Mg <sub>3</sub> (Sb, Bi) <sub>2</sub>	MgAgSb	61.0	-	Zhang <i>et al.</i> <sup>[8]</sup>

## 12. The simulated cooling performance of the 7 pairs $\text{Ag}_2\text{Se}/(\text{Bi}, \text{Sb})_2\text{Te}_3$ thermoelectric cooler

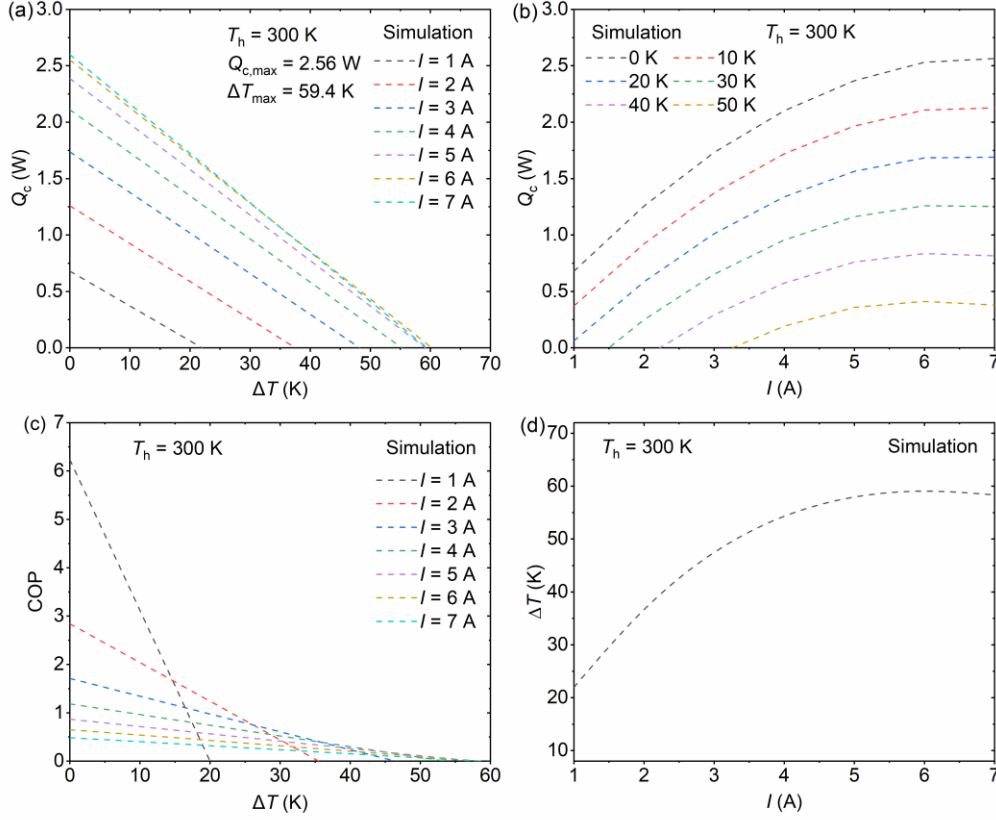


**Figure S9. The simulated cooling performance of the 7 pairs  $\text{Ag}_2\text{Se}/(\text{Bi}, \text{Sb})_2\text{Te}_3$  thermoelectric cooler.** Cooling power as a function of (a) the temperature difference at different electrical currents and (b) electrical current at different temperature differences. (c) The coefficient of performance as a function of the temperature difference at different electrical currents. (d) The maximum cooling temperature difference at different electrical currents.

### 13. Thermoelectric cooling performance of the Ag<sub>2</sub>Se-based cooler at the hot-side temperature of 325 K

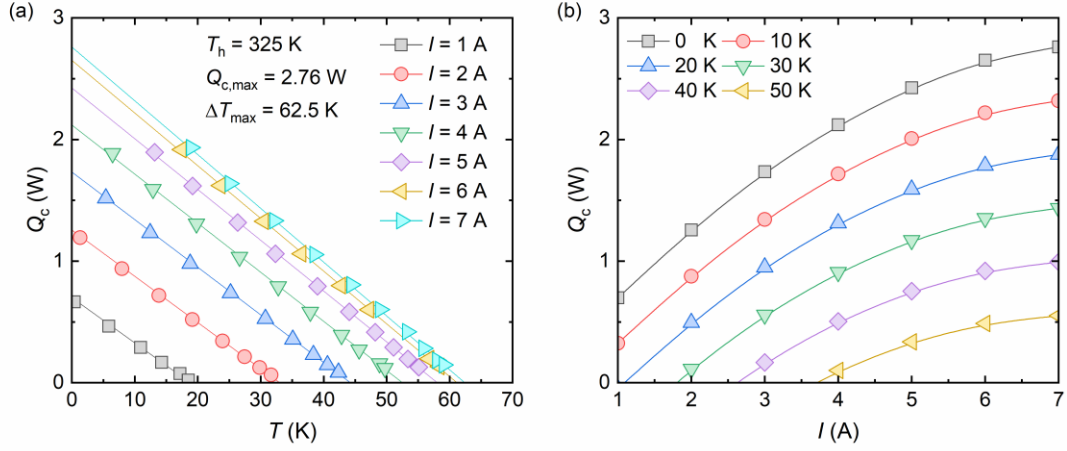


**Figure S10.** Cooling power as a function of (a) cooling temperature difference at different electrical currents, and (b) electrical current at different cooling temperature differences.

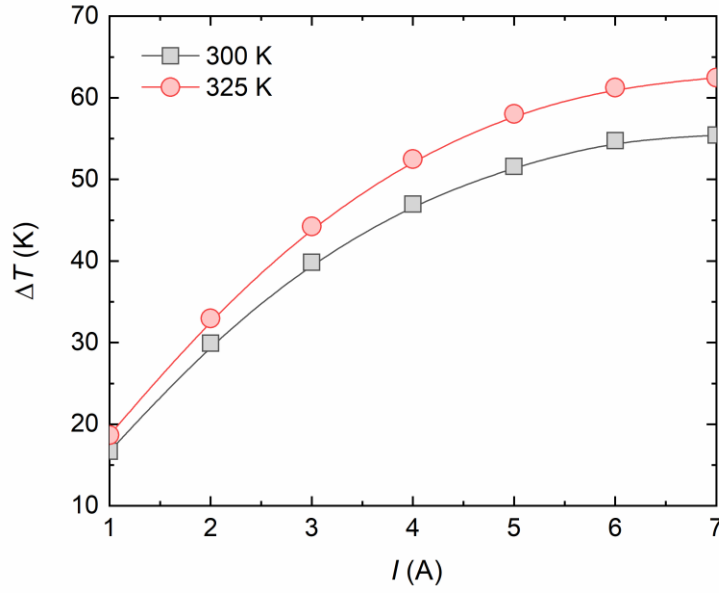


**Figure S11.** The relationship between cooling temperature difference and electrical current at the hot-side temperature of 300 and 325 K.

**14. Coefficient of performance as a function of the electrical current of the  $\text{Ag}_2\text{Se}$ -based thermoelectric cooler**

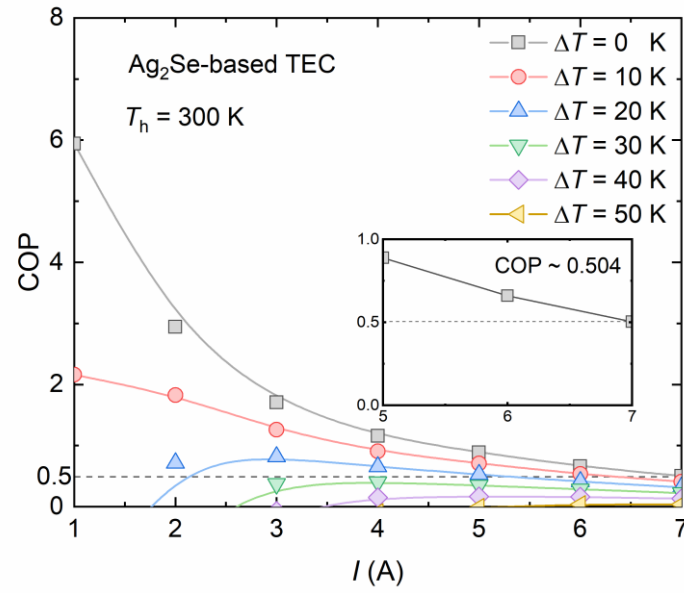


**Figure S12.** Coefficient of performance as a function of the electrical current of the  $\text{Ag}_2\text{Se}$ -based thermoelectric cooler at the hot-side temperature of 300 K.



## 15. Interfacial properties of the $\text{Ag}_2\text{Se}$ -based thermoelectric cooler after cycling

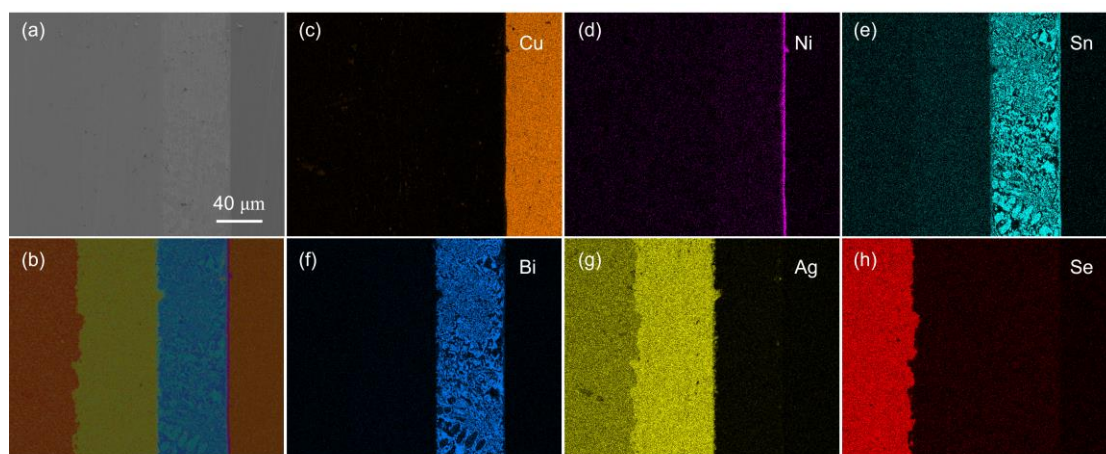


**Figure S13.** (a) Interfacial morphology, and (b-h) energy dispersive spectroscopy mapping of the interface of the  $\text{Ag}_2\text{Se}$ -based thermoelectric cooler.

## References:

- [1] Jiang F, Lin CH, Cheng JX, et al. Prefer-oriented Ag<sub>2</sub>Se crystal for high-performance thermoelectric cooling. *Adv Funct Mater.* (2024);35(6):2415000. doi: 10.1002/adfm.202415000
- [2] Liu M, Zhang XY, Zhang SX, et al. Ag<sub>2</sub>Se as a tougher alternative to n-type Bi<sub>2</sub>Te<sub>3</sub> thermoelectrics. *Nat Commun.* (2024);15(1):6580. doi: 10.1038/s41467-024-50898-6
- [3] Zhao SY, Shi XL, Zhou Q, et al. Substitution energy-guided screening of diffusion barrier materials for Ag<sub>2</sub>Se-based thermoelectric coolers. *Nano Res.* (2025);18(10):94907903. doi: 10.26599/NR.2025.94907903
- [4] Sun YX, Wu H, Dong XY, et al. High performance BiSbTe alloy for superior thermoelectric cooling. *Adv Funct Mater.* (2023);33(28):2301423. doi: 10.1002/adfm.202301423
- [5] Zhang Y, Xu G, Nozariasbmarz A, et al. Thermoelectric cooling performance enhancement in BiSeTe alloy by microstructure modulation via hot extrusion. *Small Sci.* (2023);4(2):2300245. doi: 10.1002/smssc.202300245
- [6] Ma XJ, Lin CH, Yang HY, et al. Elevating thermoelectric performance in the sub-ambient temperature range for electronic refrigeration. *Innovation.* (2025);6(5):100864. doi: 10.1016/j.xinn.2025.100864
- [7] Xie LJ, Yang JW, Liu ZY, et al. Highly efficient thermoelectric cooling performance of ultrafine-grained and nanoporous materials. *Mater Today.* (2023);65(4):5-13. doi: 10.1016/j.mattod.2023.03.021
- [8] Zhang XF, Zhu HT, Dong XJ, et al. High-performance MgAgSb/Mg<sub>3</sub>(Sb,Bi)<sub>2</sub>-based thermoelectrics with  $\eta = 12\%$  at  $T \leq 583\text{K}$ . *Joule.* (2024);8(12):3324-3335. doi: 10.1016/j.joule.2024.08.013